Oil & Natural Gas Technology

DOE Award No.: DE-FC26-06NT43067

Couple Gas/Water Interface Dynamics with Fracture Propagation (Task 6 Technical Report)

Mechanisms Leading to Co-Existence of Gas and Hydrate in Ocean Sediments

Submitted by:
The University of Texas at Austin
1 University Station C0300
Austin, TX 78712-0228

Prepared for:
United States Department of Energy
National Energy Technology Laboratory

February 23, 2009

Office of Fossil Energy

Mechanisms Leading to Co-existence of Gas and Hydrate in Ocean Sediments

Task 6: Couple Gas/Water Interface Dynamics with Fracture Propagation

for

U.S. Department of Energy
National Energy Technology Laboratory
DOE Award DE-FC26-06NT43067

by

Ruben Juanes
Department of Civil and Environmental Engineering
Massachusetts Institute of Technology
77 Massachusetts Avenue, Room 48-319
Cambridge, MA 02139
Phone: 617-253-7191, Fax: 617-258-8850
Email: juanes@mit.edu

Steven L. Bryant
Department of Petroleum and Geosystems Engineering
The University of Texas at Austin
One University Station, Mail Stop C0300
Austin, TX 78712
Phone: 512-471-3250, Fax: 512-4719605
Email: Steven_Bryant@mail.utexas.edu

February 20, 2009

TABLE OF CONTENTS

List of Figures

List of Acronyms

DEM	Discrete Element Method
LSM	Level Set Method
PFC	Particle Flow Code (commercial trademark)
PQS	Progressive Quasi-static

List of Symbols

C	curvature
$\boldsymbol{d}_i$	displacement of grain i
$\boldsymbol{f}_i$	unit vector in the direction of $\boldsymbol{F}_i$
$\boldsymbol{F}_i$	pore-pressure force onto grain i
k_0	coefficient in the kinetic model
$\boldsymbol{n}$	normal vector to a surface
r	grain radius
R_f	rigid fraction coefficient in the kinetic model

Greek letters

Γ_i	boundary of grain i
Γ_{Gi}	boundary of grain i in contact with gas

1 SUMMARY

A fundamental premise of this research project is that methane hydrate growth in sediments is dictated by the nature of the gas/water interface [Behseresht et al., 2008b]. In ocean sediments, the nature of the interface will depend critically upon the competition between grain-mechanics-controlled sediment displacement (sediment fracturing—Task 4 [Jain and Juanes, 2008]) and capillarity-controlled meniscus movement (drainage and imbibition—Task 5 [Behseresht et al., 2008a]). In this Task, we have coupled two first-principles models of these processes in order to determine when fracturing is favored over capillary invasion, and vice versa. The overarching objective of this Task was to determine whether the methodology and approach developed in Budget Period 1 of the project was a sufficient basis for continuing the research into Budget Period 2.

This task yielded two completely novel aspects. One is the accurate consideration of true multiphase flow effects in the grain displacement mechanics. Surface tension prevents that fluid pressures be dissipated quickly. Therefore, the gas pressure may be much higher than the water pressure. The difference between the two may not be sufficient to overcome the capillary entry pressure to invade a pore throat (locally), but the associated forces may be sufficient to open up fractures within the sediment.

The second is the behavior of a capillarity-dominated displacement with movable grains. This previously unstudied phenomenon reveals that the percolation behavior that characterizes capillary displacements is much less pronounced when grains can be moved by the difference between gas and water pressures. Consequently, gas is less likely to displace water down to residual saturation. This leads to a gas/water configuration more conducive to methane hydrate formation.

Based on our findings to date, we believe that these models and methodology are a solid foundation for testing the implications of our hypothesis, that is, for modeling the growth of methane hydrates from the gas/water interface locations predicted with the coupled grain-scale models. We therefore recommend that the project proceed into Budget Period 2 per the original proposal.

2 SCOPE OF THE REPORT

In Task 4 we developed a computational model that allows us to investigate the initiation and propagation of fractures in granular media [Juanes and Bryant, 2008]. The model was built in the framework of an existing discrete element method (DEM) code, PFC2D [ITASCA, 2004]. The key ingredient of the new grain-scale model developed in Task 4 is the explicit account of capillarity. The model incorporates the two-way coupling between grain dynamics and two-phase flow, by introducing two sets of forces: (1) bulk fluid forces (either water or gas); and (2) surface tension forces (due to the presence of gas–water interface).

The coupled model permits investigating an essential process that takes place at the base of the hydrate stability zone: the upward migration of methane in its own free gas phase. We elucidate the way in which gas migration may take place: (1) by capillary invasion in a rigid-like medium; and (2) by initiation and propagation of a fracture. The significant contribution of our coupled model is that it captures both phenomena and, as a result,

allows us to study the transition between the two regimes.

The model presented in Task 4, however, makes simplifying assumptions with regard to the geometry of the gas–water interface, and the resulting fluid forces and surface-tension forces onto the grains [Juanes and Bryant, 2008]. In Task 5 [Bryant and Prodanovic, 2008], invasion percolation simulation of drainage, then of imbibition, is performed, using a novel level-set method (LSM) progressive quasistatic (PQS) algorithm. The simulations provide the detailed geometry of the gas–water interface at each step of drainage or imbibition. This was performed on model sediments, as well as on a rough fracture [Karpyn and Grader, 2007]. Precise knowledge of the gas–water interface geometry is important to accurately determine bulk fluid and interfacial forces on the grains.

In this Task, we combine the modeling capabilities developed under Tasks 4 and 5. The essence is to couple the rigorous grain-scale deformation mechanics from DEM with the accurate evolution of the gas–water interface during drainage. In Section 3 we present a simplified model in which the mechanical calculations are replaced by a kinematic rule for grain displacements. In Section 4 we present the fully dynamic coupled model.

3 A KINEMATIC COUPLED MODEL

To examine the behavior emerging from competition between fracture propagation and drainage, we implemented a simple kinematic model of grain displacement during gas phase invasion of a sediment. This approach does not have the rigorous mechanics of the DEM code; it serves to illustrate the kind of behavior that may emerge.

3.1 Model Description

The PQS algorithm was modified so that grains touching the gas/water interface can be moved a short distance. To simulate grain mechanics, we introduce the following steps after each PQS drainage step:

1. Identify grains in contact with non-wetting phase.

2. The non-wetting fluid (gas) exerts force, the vector sum of which we denote $\boldsymbol{F}_i$, on each grain i identified in step 1. We assume an "elastic membrane" model, such that locally the force is normal to the fluid-grain contact (see Fig. 1). To obtain $\boldsymbol{F}_i$, we integrate the normal vector $\boldsymbol{n}$ (pointing outwards from the gas phase) along the part Γ_{Gi} of the entire grain perimeter (surface) in contact with gas. The then find the unit vector $\boldsymbol{f}_i$ in the same direction as $\boldsymbol{F}_i$.

3. Compute a displacement $\boldsymbol{d}_i$ in response to the force computed in step 2. The force is maximum when Γ_{Gi} is half-circle (half-sphere) so we set $\boldsymbol{d}_i = 4r(1-r)k_0\boldsymbol{f}_i$, where r is ratio of the lengths (areas) of Γ_{Gi} and of the entire Γ_i, and k_0 is a pre-set constant.

4. The center of grain i moves by $\boldsymbol{d}_i$ determined in step 3, but only if it will not overlap substantially with any other grains in its new position. By "substantially" in this work we mean that the distance between the grain centers would be less than a fraction R_f of the sum of their respective radii (this was set to 0.8 for most of the simulations).

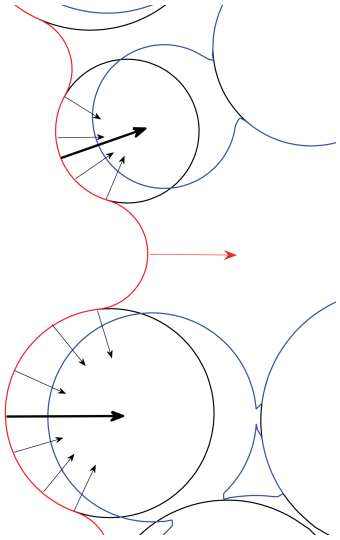

Figure 1: Schematic of a kinematic model of sediment movement driven by capillary pressure difference. Non-wetting fluid interface is shown in red and the initial grain position is shown in black. Small black arrows show the normal vectors along the contact line between non-wetting fluid and grain surface. Enlarged black arrows show their (integral) direction and consequently the direction of grain movement. New grain positions are outlined in blue.

This procedure does not consider the forces imposed by neighboring grains, which are the essence of the solid mechanics; this is the proper role of DEM described in the next section. Thus we do not attempt to determine the exact magnitude of $\boldsymbol{F}_i$, nor the exact displacement $\boldsymbol{d}_i$ from Newton's Second Law. The kinematic approach simply provides insight into the type of behavior that can arise from the coupled displacements.

3.2 Model Application

The nature of the resulting gas/water drainage displacement is significantly different than when the grains are fixed.

We illustrate the coupled behavior in two 2D packs of circular grains. The first one was obtained by packing disks of unit radius on a regular triangular grid except for one disk that was slightly offset (see Fig. 2). Drainage curves (Fig. 10) show remarkable qualitative and quantitative differences for this simple medium due to coupling of fluid and sediment movement. In the case of stationary grains (not shown), almost all the pore throats are the same size and thus almost the entire domain drains quite suddenly when the applied curvature increases to 11. When fluid pressure displaces the grains, Fig. 2, the domain begins to drain at much smaller curvatures, the percolation threshold is much less sharp, and the irreducible wetting saturation is larger. The first of these three observations makes intuitive sense: moving grains apart decreases the critical curvature required to force a meniscus between them. Less obvious are the second and third observations. Behind the advancing gas phase, grains are pushed into each other, narrowing the pore throats between them. This increases the pressure required to invade the undrained region behind the leading edge of the advancing front. Thus the drainage curve is smoothed out in the coupled displacement.

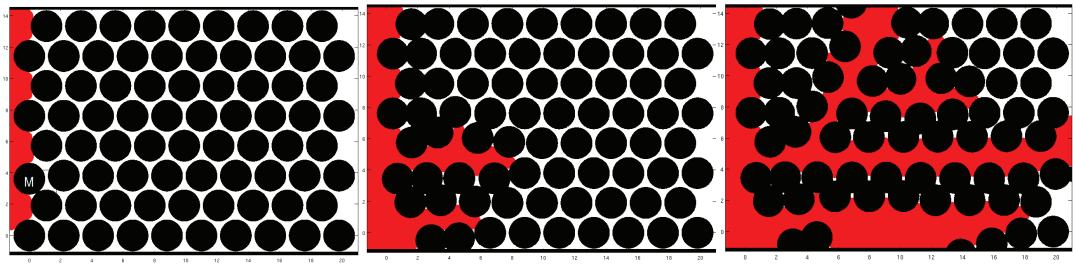

Figure 2: (Left) Nonwetting fluid at the first step of PQS simulation is shown in red, $C = 2.36$. The spheres (in black) form a regular packing (except for one sphere in the first column—marked by letter M—that is offset slightly) and have not moved yet. (Center) Nonwetting fluid at $C = 6.36$ of the coupled PQS simulation. The packing "irregularity" has, under- coupled fluid and sediment movement, triggered an opening of two fluid pathways. (Right) Fluid/sediment configuration at the point where fluid percolates to the other side ($C = 8.56$).

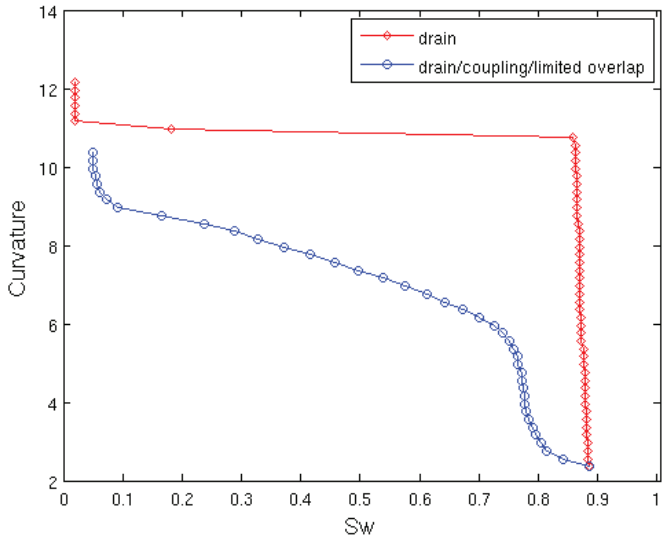

Figure 3: Comparison of curvature-wetting fluid saturation curves for drainage in the regular packing of disks with and without coupling. Note that the initial packing has basically only two throat sizes. Thus if the grains are stationary, once curvature is high enough to drain the smaller throats, the whole rest of the domain drains. This yields a characteristic single large jump in the corresponding C–S_w curve.

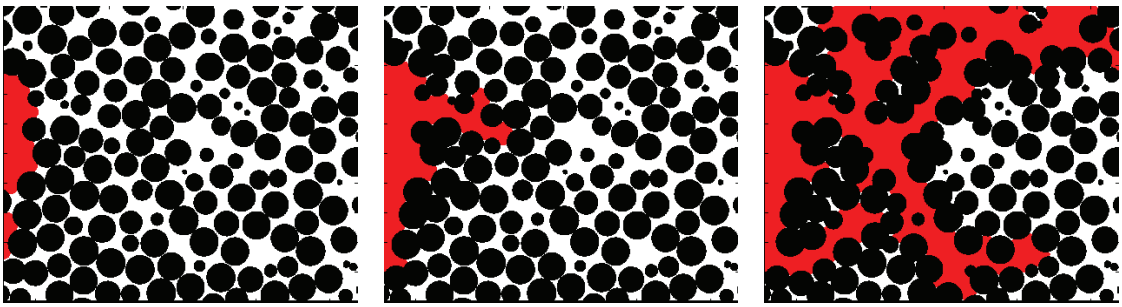

Figure 4: (Left) Nonwetting fluid at the first step of PQS simulation is shown in red ($C = 2.48$). The spheres (in black) have not moved yet. (Center) Nonwetting fluid at $C = 3.68$ of the coupled PQS simulation. The fluid has opened a pathway, which just started to split into two. (Right) Fluid/sediment configuration at $C = 6.08$ where fluid percolates to the other side for the first time.

The second geometry is a cross-section of the Finney pack [Finney, 1970] resulting in a close packing of disks with radius 1.0 or less (Figs. 4 and 5). We removed three disks at the entrance to create a preferred region for onset of grain displacement. The displacement becomes self reinforcing: moving grain decreases the curvature required for drainage to occur, leading to gas invasion that moves grain apart in the invaded pore.

We have applied this procedure to three-dimensional packs as well. We also observe dramatic differences between the fixed-grain and moveable-grain models. If the grains in the sediment are randomly arranged and fixed (see Fig. 6), gas invasion forms a highly ramified structure (familiar percolation branching in sediments). On the other hand, if the same grains are movable, gas invasion forms channels (see Fig. 7).

If sediment grains are (locally) ordered (Fig. 8) and movable, gas invasion form fracture-like patterns oriented by the original ordering (Fig. 9). The extent to which these patterns emerge depends on the softness of the sediment (measured by coefficient R_f, the rigid fraction of each grain) and how rapidly grains can be displaced (relative to the rate of increase of the capillary pressure, measured by coefficient k_0); see Fig. 10.

Movable grains also change the gas/water displacement quantitatively. Drainage occurs at lower curvatures, and can be much more gradual at intermediate rates of grain displacement. The morphology and amount of residual wetting phase change substantially: larger quantities of water are held in pores behind throats narrowed by overlapping displaced grains (see Fig. 11). The area of the gas/water interface is smaller.

Capillarity-controlled gas invasion of a hydrate stability zone can occur at smaller gas pressures if the sediment grains are movable. This alters the competition between drainage and fracture initiation by gas pressure. It also shifts the likely growth habit away from grain-cementing toward pore-filling, if growth starts at a drainage endpoint. Perhaps most importantly, grain displacement during drainage brings about the possibility of a structural growth habit, wherein the hydrate forms part of the load-bearing matrix. This cannot occur in fixed-grain drainage.

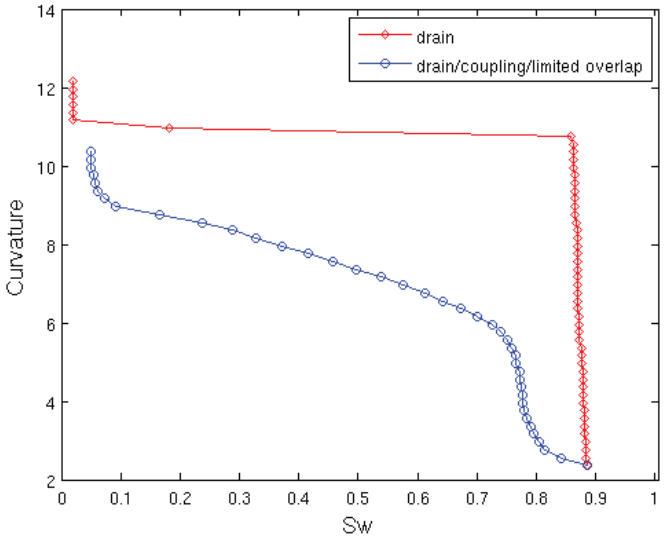

Figure 5: Comparison of curvature-wetting fluid saturation curves for drainage in the cross section of the Finney pack with and without coupling.

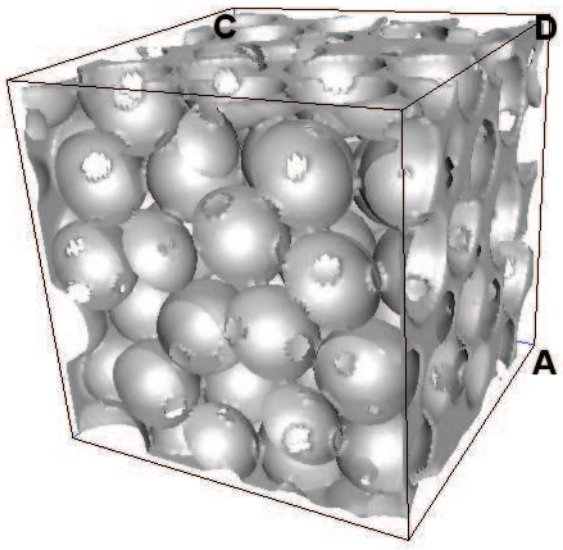

Figure 6: Pore-grain surface of a subset of a close, random packing of equal spheres. Drainage started from the face ACD towards the viewer. The volume sides orthogonal to the main displacement direction were closed, and the other two were open for gas phase entry and water phase exit.

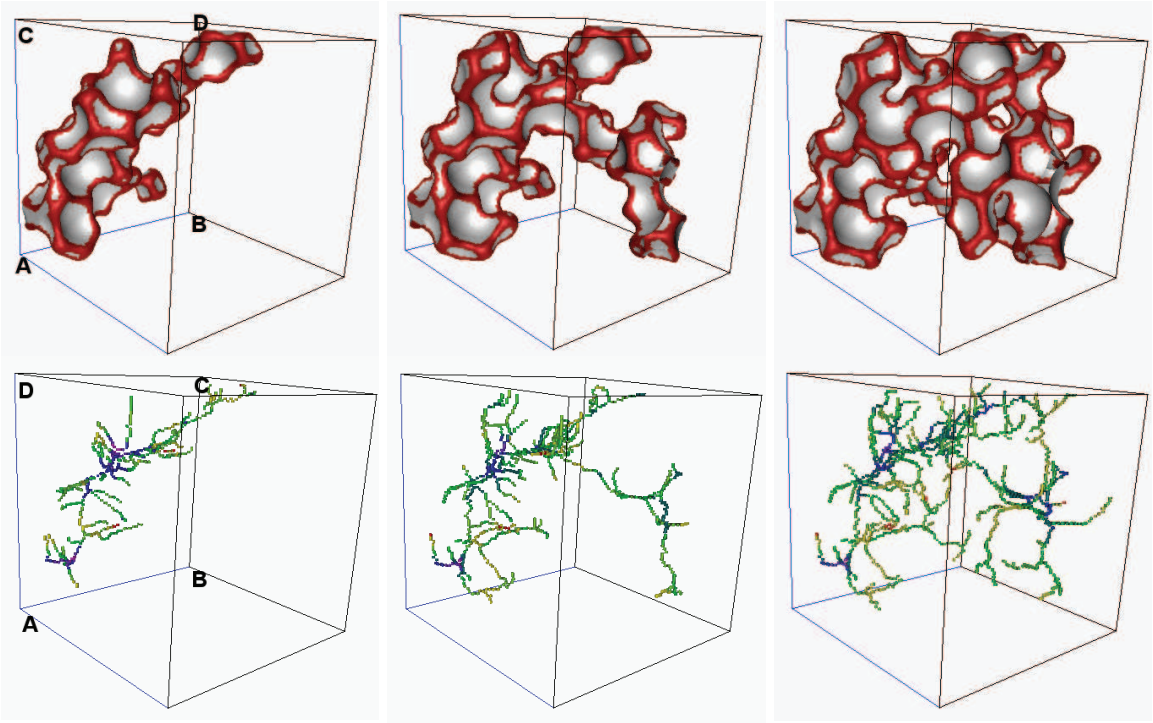

Figure 7: LSMPQS drainage with movable grains in random close packing subset: top view non-wetting fluid phase at a sequence of steps with standard coloring (red for fluid–fluid and gray for fluid–grain contact). Nonwetting fluid enters from the face marked ABCD. Bottom view shows medial axis corresponding to the non-wetting phase for each step. (a) Just before percolating. (b) At the point when fluid percolated to the opposite volume side, $C_6 = 5.38$, we observe a single pathway across the volume. (c) Just after percolating, $C_7 = 5.58$, no specific fracture-like opening is observed.

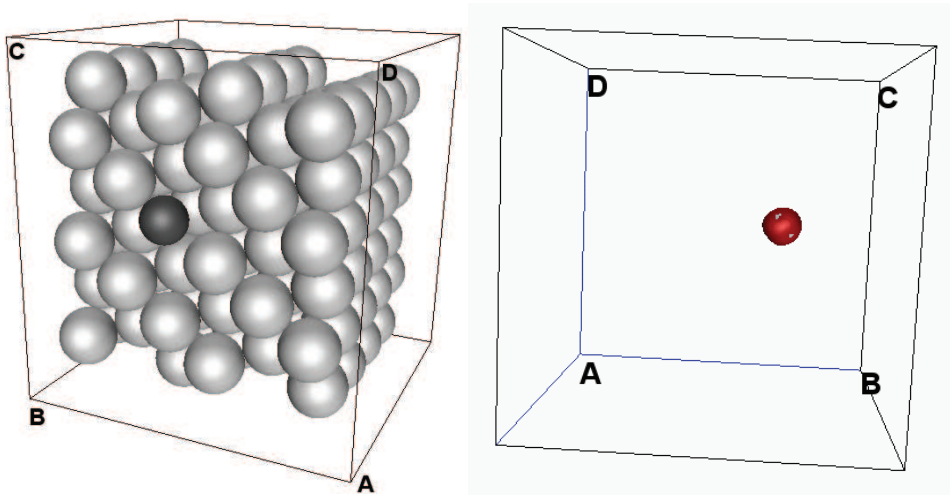

(a) (b)

Figure 8: (a) Spheres in (regular) hexagonal close packing with a defect. The darker sphere has been slightly moved from the regular position, and its radius reduced to create an entry point for invading gas phase. (b) Non-wetting phase surface (its contact with wetting fluid is shown in red, and its contact with grain—very small in this case—is in gray). The initial step of drainage (resulting from a slightly compressible model, $C_1 = 4.05$) in the regular packing with a defect. Since (a) and (b) images are different rotational views, we have marked the entry face for simulation ABCD.

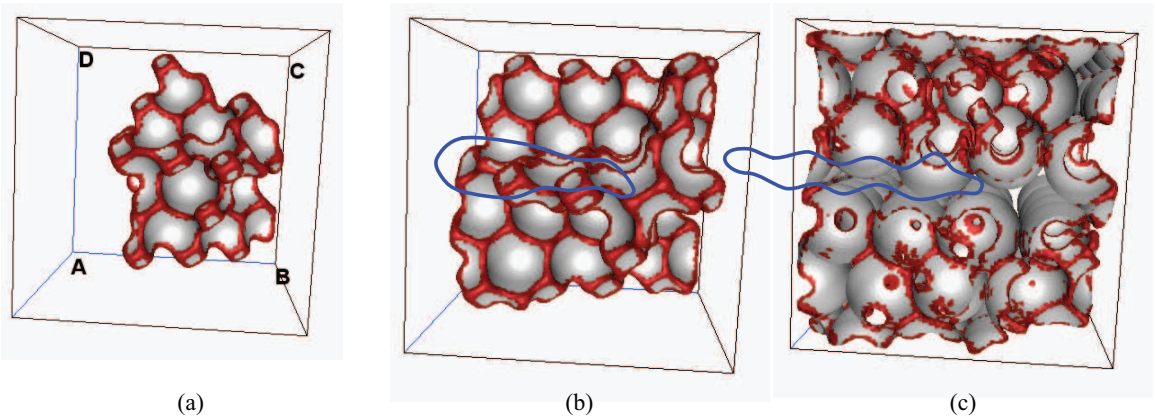

(a) (b) (c)

Figure 9: LSMPQS drainage of the almost-regular packing of Fig. 8 when grains can be displaced by net force from the gas phase. Coefficients used were $k_0 = 2$ and $R_f = 0.8$. From left to right the frames show a front view of the gas phase at steps $C_{12} = 6.25$, $C_{18} = 7.45$ and $C_{48} = 13.45$ (final step). Gas enters from the face marked ABCD in the rear and moves towards the viewer. The gas-brine interface is in red, and the gas-grain is in gray. The blue curves indicate fracture-like openings created as gas displaces grains. Grain displacement is evident most clearly in the rightmost frame, where large-diameter pendular rings of brine surround contacts between grains that have been pushed into overlap.

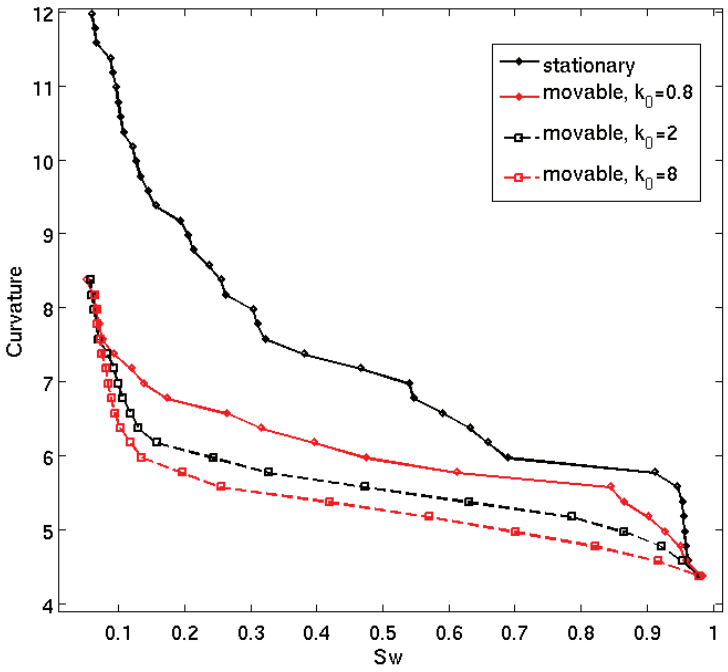

Figure 10: Comparison of simulated drainage curves in close, random packing (see Figs. 6 and 7) with stationary and movable grains, with different coefficients k_0 that measures how rapidly grains can be displaced. The rigid fraction (fraction of each grain that is impenetrable by other grains) was kept constant at $R_f = 0.8$.

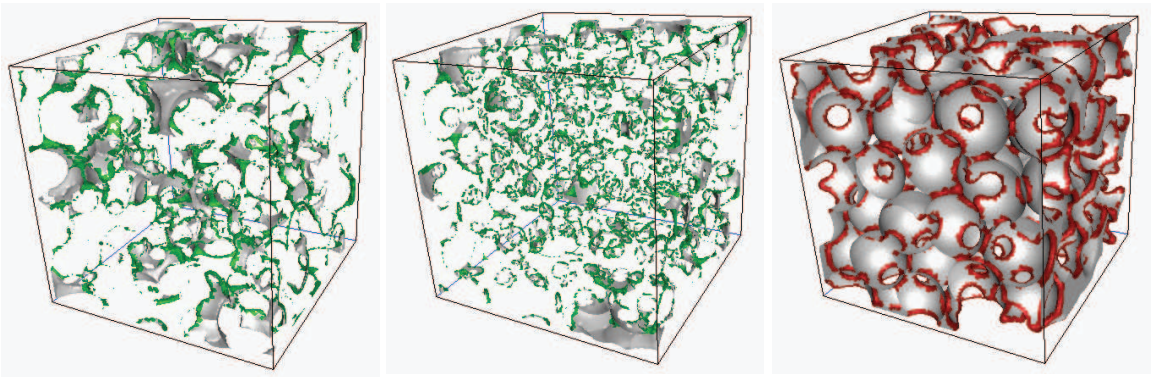

Figure 11: (a) Wetting fluid configuration corresponding to Fig. 7c. Fluid-fluid interface in this plot is green, and the wetting fluid-grain contact is in gray. (b) Wetting fluid configuration at the end of drainage with stationary grains, same color scheme as in (a). (c) Nonwetting fluid configuration at the end of drainage with stationary grains that corresponds to (b).

4 A FULLY DYNAMIC COUPLED MODEL

4.1 Model Description

We describe the rigorous coupling of the level set method/progressive quasistatic (LSMPQS) model for capillarity-controlled displacement and the discrete element method (DEM) code for displacements driven by grain mechanics, fluid pressures and surface tension.

The general approach to the coupling of LSMPQS and DEM is as follows. We determine an initial configuration of the granular sample, usually by simulating sedimentation and compaction as described in detail in Task 4. We load the packing by setting one or more of the pores as being filled with gas. From this initial configuration of the packing geometry we compute gas–water interfaces with the level set method (see Task 5). From these, the calculation will provide pore fluid forces and capillary forces in pendular rings. These forces are applied in the mechanical equilibrium calculation using PFC—see Task 4 for a detailed description of the formulation. After the mechanical step, the geometry of the packing may change due to fracture opening, or other grain displacements. With the updated geometry, new critical curvatures are calculated, and used to drive gas–water interfaces to a new equilibrium.

In the framework that we implemented, the two processes—interface evolution, and grain dynamics—are explicitly coupled.

4.2 Model Application

We apply the rigorous coupled model to the same simulation set-up used in Task 4. We create a sample of 300 grains of grain size $[r_{\min}, 2r_{\min}]$, which settle by gravity. The sediment is compacted under constant pore pressure (drained conditions) until a desired confining stress is achieved. We impose an anisotropic stress state, with effective stresses $\sigma'_v = 10$ kPa, and $\sigma'_h \approx 8$ kPa. The interfacial tension is $\gamma = 50 \times 10^{-3}$ N/m. We assume that the cohesion is inversely proportional to grain radius. This is phenomenologically adequate (fine-grained material like clays are cohesive) and is also consistent with the adhesive forces that result from the presence of a gas–water interface [Orr et al., 1975; Kato et al., 2004]. The only parameter that is left free is the grain size $r_{\min}$.

In Task 4 we already showed that the grain size is the critical parameter determining the mode of gas invasion (capillary invasion or fracturing opening). Here, we illustrate the application of our coupled DEM–LSMPQS model to a sample that will develop a fracture. We choose $r_{\min} = 1$ μm.

The initial configuration is shown in Fig. 12(a). We compute the gas configuration and the forces exerted by gas on grains in contact using the LSMPQS algorithm. The DEM grain-grain contact force network is augmented by gas forces and grains move accordingly. This process is iterated, as capillary pressure increases, see Fig. 12(b)–(f).

It is interesting to compare the result of the rigorous coupled DEM-LSMPQS model, with that of the DEM model developed in Task 4. The latter features the full mechanics, but simplified calculations of pore-pressure forces and capillary entry pressures. For this case, both models produce similar—but not identical—results. The fully coupled model predicts that the fracture branches into two fractures during its evolution, whereas the DEM model

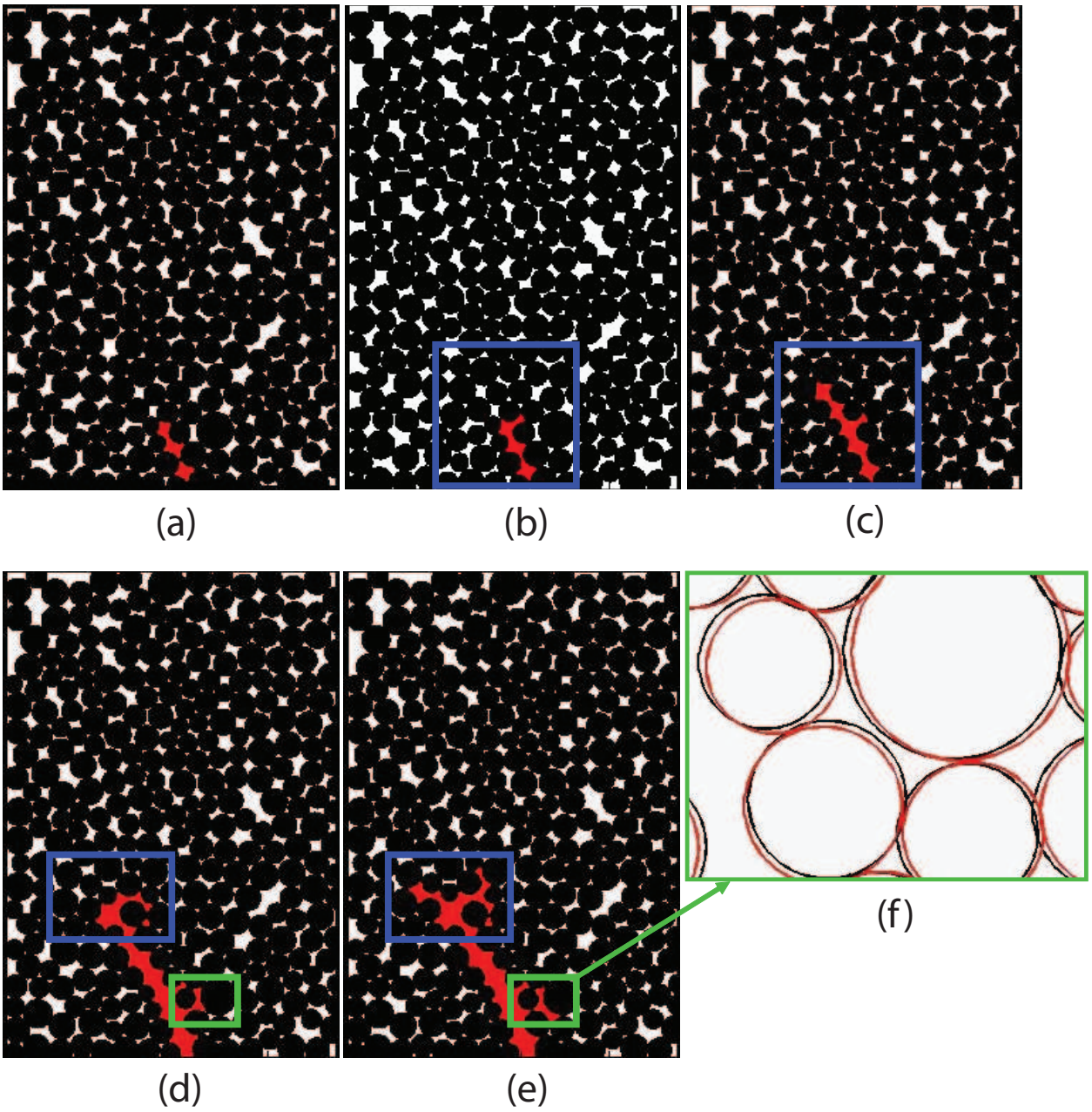

Figure 12: Gas invasion by fracturing, computed with the coupled DEM-LSMPQS model developed in this Task. Shown are several stages of the invasion process. (a) Initial gas configuration for coupling. Gas injected into three selected pores and the configuration shown in red is the result of the PQS algorithm. Had grains been unable to move, that would be the end of invasion (packing is tight). (b)–(c) Gas pathway opens up between two consecutive (coupled) steps. (d)–(e) Further (consecutive) steps of simulation that show gas pathway starts branching (blue) as well as some gas getting trapped by grain movement (green). (f) The close up figure shows grain interfaces before (black) and after (red) they moved in consecutive steps.

predicts a single growing fracture. The movies comparing the results of both simulations are attached to this report as supplementary material.

REFERENCES

J. Behseresht, Y. Peng, M. Prodanovic, and S. L. Bryant. Pore-scale mechanistic study of the preferential mode of hydrate formation in sediments: Role of capillarity. In *Proc. 6th Intl. Conf. Gas Hydrates (ICGH 2008)*, Vancouver, Canada, July 6–10, 2008a.

J. Behseresht, Y. Peng, M. Prodanovic, S. L. Bryant, A. K. Jain, and R. Juanes. Mechanisms by which methane gas and methane hydrate coexist in ocean sediments. In *Offshore Technology Conference*, Houston, TX, May 5–8, 2008b. (OTC 19332).

S. L. Bryant and M. Prodanovic. Mechanisms leading to co-existence of methane gas and hydrate in ocean sediments. Task 5: Compute grain-scale gas/water geometry, U.S. Department of Energy, DOE/NETL Grant DE-FC26-06NT43067, October 2008.

J. L. Finney. Random packings and the structure of simple liquids. I. The geometry of random close packing. *Proc. Roy. Soc. Lond. A*, 319:479–493, 1970.

ITASCA. *PFC2D, v3.1 – Theory and Background.* Itasca Consulting Group, Inc., Minneapolis, MN, 2004.

A. K. Jain and R. Juanes. Pore-scale mechanistic study of the preferential mode of hydrate formation in sediments: Coupling of multiphase fluid flow and sediment mechanics. In *Proc. 6th Intl. Conf. Gas Hydrates (ICGH 2008)*, Vancouver, Canada, July 6–10, 2008.

R. Juanes and S. L. Bryant. Mechanisms leading to co-existence of methane gas and hydrate in ocean sediments. Task 4: Fracture initiation and propagation, U.S. Department of Energy, DOE/NETL Grant DE-FC26-06NT43067, May 2008.

Z. T. Karpyn and A. S. Grader. Visualization of fluid occupancy in a rough fracture using micro-tomography. *J. Colloid Interface Sci.*, 307:181–187, 2007.

S. Kato, T. Sakakibara, and H. Yoshimori. Effects of intergranular adhesive force on behavior of granular material. In Y. Shimizu, R. D. Hart, and P. Cundall, editors, *Numerical Modeling in Micromechanics Via Particle Methods. Proc. of the 2nd International PFC Symposium, Kyoto, Japan*, pages 347–354, Balkema, Leiden, October 2004.

F. M. Orr, L. E. Scriven, and A. P. Rivas. Pendular rings between solids: meniscus properties and capillary force. *J. Fluid Mech.*, 67:723–742, 1975.

National Energy Technology Laboratory

626 Cochrans Mill Road
P.O. Box 10940
Pittsburgh, PA 15236-0940

3610 Collins Ferry Road
P.O. Box 880
Morgantown, WV 26507-0880

One West Third Street, Suite 1400
Tulsa, OK 74103-3519

1450 Queen Avenue SW
Albany, OR 97321-2198

2175 University Ave. South
Suite 201
Fairbanks, AK 99709

Visit the NETL website at:
www.netl.doe.gov

Customer Service:
1-800-553-7681